Journal Title
XX(X):1–12

DOI: 10.1177/ToBeAssigned
www.sagepub.com/
SAGE

Experimental characterization of fused filament fabrication printed parts under tension, shear and combined shear-tension loads via Arcan test

Isaac Ferreira[1,2], Abílio Jesus[1,2], Margarida Machado[2], João Pereira[2], Jorge Lino Alves[1] and José Xavier[3]

Abstract

The mechanical performance of fused filament fabrication (FFF) printed parts is considered the weak point of the technology due to its high anisotropic structure and irregular behaviour. This research focuses on the application of the Arcan based method to FFF printed parts, to better understand their mechanical behaviour. In order to characterize and quantify the anisotropic behaviour, a butterfly type specimen was developed, taking into account the flaws presented by the process (e.g. need for support material for tilted surfaces, low resolution, etc.). Together with the Arcan type grip, a combination of vertical - transversal (VT), vertical-longitudinal (VL) and horizontal (H) printed samples were tested under three distinct loading conditions, 90° - tensile, 45° - combined loading and 0° - pure shear. For each set of samples, digital image correlation (DIC) was used to analyse the deformation fields imposed by the distinct building orientations and loading conditions. Regarding the material, two different types of Nylon®(PA 12) were used, namely FX256 and CF15, being the second a short carbon fibre reinforced version of the first, allowing a comparison of the mechanical behaviour. The results show that the building orientation prevails, originating distinct fracture types and overall behaviour difference. It was shown that fibre presence does not create a stronger material, yet an increase in stiffness is observed for all building orientations, except VT, where both materials presented similar values, indicating that the fibre orientation is critical when taking into account the loading conditions. It was also observed that of all sample types, FX256 H specimens showed the closest to isotropic behaviour.

Keywords

FFF, Additive manufacturing, PA12, composites, short fibre, Arcan, Mechanical behaviour

Introduction

Similarly to traditional composites, AM produced parts, particularly FFF manufactured parts, if considering the production orientation or internal parametrization, present an anisotropic mechanical behaviour. Due to its in planar infill strategy, the mechanical performance may vary according to the selected property, indicating that anisotropy is present even at layer level. Correspondingly to traditional laminate composites, AM parts are built layer-by-layer. Unlike most traditional composite conformation methods in which shell type parts are obtained, AM/FFF parts are built in a layer-wise manner until an enclosed 3D shape is obtained. Therefore, building directions must be considered in the design stage. Functional parts produced by this technology be subjected to different loading in distinct directions, also resulting distinct mechanical responses. Anisotropic behaviour related to internal pattern and building orientation is characteristic of AM produced parts. Consequently, it is of the most importance understanding the effects caused by these parameters on the part final performance.

Koch *et al.* (2017) focused their study on the evaluation of the impact in mechanical performance caused by the use of three distinct infill patterns - 0° (longitudinal, concentric samples), ±45° (alternate, diagonal) and 90°(transverse samples) - when compared with injection moulded tensile specimens using acrylonitrile butadiene styrene (ABS) material. In addition, the compaction rate effect (caused by bed adjustment parameters) on the mechanical performance of the specimens was evaluated. The tests indicate that the tensile strength of longitudinal samples was 92.3% of the injected material, while the worst behaviour was presented by the transversally printed samples, with 72% of the injected parts tensile strength. It is demonstrated that high compaction levels lead to improved mechanical results. Jiang & Smith (2017) studied the anisotropic mechanical properties of carbon filled feedstock by printing tensile samples according to 0°, ±45° and 90° infill orientations. Beyond the infill strategies, a comparison was also made with the unreinforced versions of each material. The results showed that beyond the increase in mechanical strength due to the fibres presence, the best behaviour was always

[1]Faculty of Engineering, University of Porto, Portugal
[2]INEGI, Porto, Portugal
[3]UNIDEMI, Department of Mechanical and Industrial Engineering, NOVA School of Science and Technology, Universidade NOVA de Lisboa, 2829-516 Caparica, Portugal

Corresponding author:
Isaac Ferreira, FEUP, Faculty of Engineering, University of Porto, Porto, Portugal.
Email: iaferreira@inegi.up.pt

observed in the longitudinal direction. Similar results were also found by Ahn *et al.* (2002) and Casavola *et al.* (2016), that adopted the same infill strategies. These results showed, that even in xy plane, distinct patterns result in different performances.

Due to its layer-by-layer nature, which is more pronounced in FFF process than other technologies, Z or upright build direction is the least favourable as regards the mechanical performance. Chacón *et al.* (2017) studied the effect of process parameters on mechanical properties by varying the layer thickness, printing orientation and speeds. Tensile samples were printed horizontally (90° - flat), on edge (90°) and upright (0°), being this way possible to quantify the differences in mechanical performance of these orientations. Tensile results showed that between the flat and on edge samples there was no significant difference in strength, even considering different layer thickness and printing speeds. However, for upright specimens, the tensile strength increased with the increasing layer thickness, indicating that, smaller layers results into less interfacial contact and higher number of interfaces. Even though, upright samples presented an average of 45% decrease in tensile strength (for the best layer thickness parameters) compared to flat samples. Rybachuk *et al.* (2017) studied the anisotropic behaviour of ABS printed parts through tensile and compressive tests. Dogbone specimens were produced horizontally (90°-flat), on edge (90°) and vertically (0°), while the compressive tests were performed with cylindrical samples printed vertically, horizontally and at 45°. It was shown that, between flat and on edge type specimens there is not relevant differences in the tensile behaviour, while the vertical specimens' tensile strength is rougly half of the previous. As concerns the compressive specimens, there is no significant changes in performance for the three orientations, indicating that compressive mechanical performance are less sensitive to the printing orientation. Zou *et al.* (2016) studied the anisotropic behaviour of tensile specimens printed upright (0°) and at angles of 30°, 45°, 60° and 90° (on edge samples), as seen in Figure 1. The results showed that the worst mechanical performance (strength) was achieved for the 0° for the same material, being increased gradually as this angle increases. The anisotropy of AM parts has been

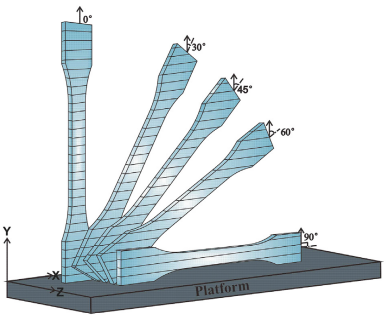

Figure 1. Specimens building orientations (Zou *et al.* 2016).

studied through different approaches, being the comparison of tensile behaviour of vertically and horizontally printed specimens the most common. However, this approach is not ideal, as the tensile samples are usually long, which implies long printing times, resulting in large thermal gradients. Beyond this, there is the fact that printing imperfections are prone to occur vertically, since the specimen in cause is not adequate for this type of operations. Therefore, it is essential to identify a type of sample that would reduce this type of problem, and allow several building directions.

The Arcan testing method (Arcan *et al.* 1978) was developed to analyse uniform combined plane-stress in fibre reinforced materials. The original developed Arcan specimen was a circular plane, with opposite cut outs and a centralized small test area. These samples were extracted from a plate, and tested on a universal test machine. A second version of the test was then developed by Voloshin & Arcan (1980), transforming the sample into a re-usable metallic apparatus or grip setup for composite samples. Currently, the Arcan test is based on two components: a specimen, which might be presented in different shapes (Hoffmann *et al.* 2015; Hachour *et al.* 2014; Xavier *et al.* 2018; Alfonso *et al.* 2018; Manaia 2018; Manaia *et al.* 2019; **?**) and two semi-circular gripping plates, holding the test sample. Each metallic grip has a set of holes which allows the apparatus to test a combination of biaxial loads such as, combined shear and tension, or just tension or pure shear (Manaia 2018; Manaia *et al.* 2020). This type of apparatus has been used to test distinct types of materials since then. Alfonso *et al.* (2018) studied the strength of bonded assemblies for automotive applications by subjecting these samples to a series of tests ranging from 0° (tensile), 45° (tensile–shear), 90° (shear) and 135° (compression–shear). Créac'hcadec *et al.* (2015) evaluated an epoxy adhesive mechanical response with a modified Arcan method for the same range of orientations. Fibre reinforced composites are the most common material tested using the Arcan apparatus. An investigation of combined-mode delamination of carbon fibre reinforced Polyetherimide (CF/PEI) samples under different stress combinations, varying the loading angle from 0 to 90° was conducted by Choupani (2008). Gning *et al.* (2010) used the Arcan apparatus to test two distinct types of glass fibre/epoxy composites, using the pure tension, shear and tension/shear loadings. Hung & Liechti (1997) analysed the shear behaviour of laminated specimens, in which the samples were cut off from a continuous carbon fibre reinforced Polyether ether ketone (AS4/PEEK) unidirectional laminate composite. Considering the literature review on testing methodologies for anisotropic materials, only limited types of data can be provided by common tensile tests. The purpose of this work is to develop a type of sample that avoids the major problems found in previous researches. Samples created in distinct build orientations and subjecting them to different types of loading combinations, are proposed to provide a better understanding of the anisotropy on the mechanical behaviour. Digital image correlation (DIC) is an optical method, capable of providing full-field displacements of a specimen through the comparison of the images captured at distinct mechanical states (Dias *et al.* 2013). Therefore, it is widely used as part of distinct types of mechanical tests, which in some of the cases the traditional contacting measurement methods are not capable (Caminero *et al.* 2012, 2014; Dias *et al.* 2013). The Arcan method is one of these types of test which could be enriched in association with DIC due to its capability to measure displacements in distinct orientations, thus being

part of this study (Xavier *et al.* 2018; Alfonso *et al.* 2018; Hachour *et al.* 2014).

To the best of the author's knowledge, this testing methodology was not yet applied to FFF printed samples. Therefore, an experimental approach for assessing the mechanical response of FFF specimens under multiaxial loadings is presented, coupling the Arcan fixture apparatus with full-field deformation measurements via DIC. An Arcan test-based geometry was designed considering the limitations of FFF process (e.g., to print wall angles greater than 45° without supports structures). Regarding the material, two compositions were used, namely polyamide 12 (PA12) and short fibre reinforced polyamide 12 (CF15). Testing samples were produced according three different build orientations namely, Horizontal (H), Vertical-Transverse (VT) and Vertical-Longitudinal (VL), and tested under three distinct loading directions, 90°- tensile, 45°- combined tensile-shear and 0°- pure shear.

Experimental details

Arcan test

The Arcan apparatus used in this study, was also applied by Manaia (2018) and it is based on the Doyoyo & Wierzbicki (2003) concept, an evolution of the original Arcan *et al.* (1978) test. As presented in Figure 2a, this setup consists of two semi-circular steel plates with clamping bars hold by a screw in each end. In order to avoid the test specimen slipping, two extra central clamps were added, allowing better pressure distribution throughout the sample. Each semi-circular plate presents an array of holes 15° apart from each other, ranging from 0 to 90°, being the 90° tensile and 0°, pure shear. Each steel plate is then fixed with machine loading axis by two pins. Considering the setup specifications, three positions were analysed for the purpose of this study, corresponding to shear (α=0°), combined tension and shear (α=45°) as well as pure tensile loading (α=90°) as presented in Figure 2b, in which a global coordinate system is also proposed.

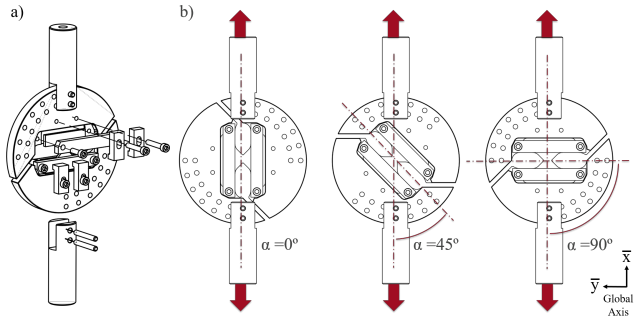

Figure 2. Arcan apparatus: (a) components and (b) selected test orientations.

As above-mentioned and depicted in figure 2a, the two-pin configuration was selected. Beyond the practicality that the rigid configuration offers in what concerns samples exchange, there is a more important benefit. Since these polymers are generally soft as compared to metals, a problem is usually observed, consisting in the deformation development localized in undesired locations of the test specimen. These deformations are generated by the rotation of the set (grips-specimen) when an angle different than α=90° is applied when a one-pin setup is utilized. Therefore, the two-pin configuration was selected. This type of assembly was previously tested by Doyoyo & Wierzbicki (2003), proving that it could overcome the lack of stress uniformity (Mohr & Doyoyo 2009).

With the butterfly specimen and Arcan setup, it is possible to analyse distinct stress combinations, in the central interest section marked in red in Figure 3. By defining a local coordinate system, in which the interest area is parallel to the Y axis and perpendicular to the X axis, it is possible to obtain mean shear stress τ_{xy} and mean normal stresses σ_{xx}, following the equations in the Analytical formulation section.

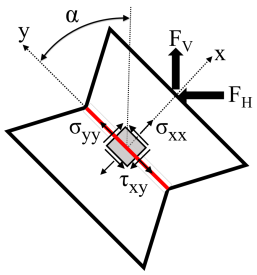

Figure 3. Biaxial state of stress at the gauge region of the test specimen, adapted from Mohr & Doyoyo (2009); Doyoyo & Wierzbicki (2003).

Test sample development

Butterfly test samples have been used in previous studies (Manaia 2018; Hachour *et al.* 2014), with this type of grips. However, these specific specimens presented a section reduction in the gauge region, which was easy to produce using injection moulding. Due to the layer-by-layer fabrication method of the current study, this gauge geometry would complicate the specimen production. Thus, an alternative butterfly shaped specimen was developed (Figure 4c), maintaining the overall external dimensions of the samples used by Manaia (2018) as demonstrated in Figure 4b. This new sample was inspired in the original Arcan geometry (Figure 4a), excluding the thickness reduction at the gauge section, and thus allowing for a simple production process.

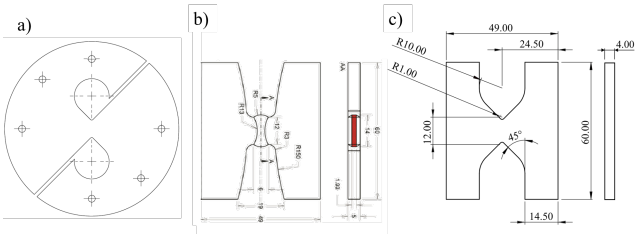

Figure 4. (a) Original Arcan sample configuration, (b) butterfly specimen (Manaia 2018) and (c) developed geometry.

The new developed specimen was subjected to Finite Element (FE) calculations using Abaqus, with four-noded plane stress quadrilateral elements with reduced integration (CPS4R), in the elastic regime. The material was assumed

as isotropic with properties as obtained previously for CF15, through tensile tests. Boundary conditions were applied to one of the sample's arm locking its x and y displacements and rotations. The sample was placed at 0°, 45° and 90°, in which a displacement was applied to the other arm, in x direction as it can be observed in Figure 5. Von Mises stresses are presented, confirming that the higher stress values are located in the notch area, thus validating the geometry for an isotropic material hypothesis.

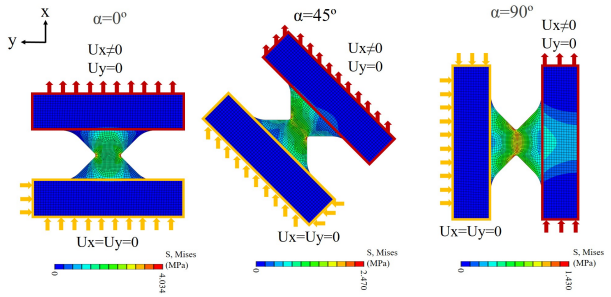

Figure 5. Von Mises stress simulation results for tensile, combined mode and shear tests.

Specimen building orientation

Taking into account the anisotropic studies presented in the literature review, the performance of FFF specimens produced according three distinct build orientations will be investigated. Figure 6 depicts the three build orientations as produced on the equipment tray. The sample 1 in Figure 6 is representative of the flat or horizontal samples denominated as H specimens, presenting an infill orientation of $\pm 45°$. Due to the flat build orientation, and alternate infill direction, these samples present, theoretically, the nearest to isotropic behaviour from the set. Samples 2 presented in Figure 6, which were built in the upright position are denominated as VT (vertical-transversal), V indicating the building orientation and T, the layer deposition orientation in a tensile loading scenario (α=90°). For this specific case, the interlayer adhesion is tested. The last type of sample (3) is denominated VL. Similarly to the previous, these specimens were printed vertically V, being rotated so that, in a tensile test scenario (α=90°), the deposition lines would be aligned with the loading axis as depicted in Figure 6.

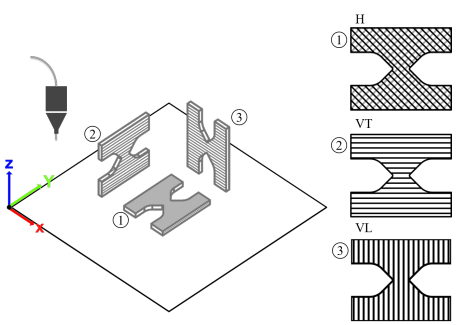

Figure 6. Specimen building orientation.

Arcan test - Analytical formulation

Considering the testing apparatus setup depicted in Figure 2a, two pins configuration was adopted, avoiding rotations of each grip; it is possible to detect that rotation movements are prone to occur for shear or combining mode tests and possible specimen misalignments. By applying the two-pins gripping, the lateral movements due to rotations are avoided, being ensured a test sample alignment with the loading axis (Manaia 2018). Nevertheless, a perpendicular to the loading direction reaction force is generated, differentiating from the one pin setup purposed by Arcan *et al.* (1978), in which this lateral reaction is converted into a rotation. To correctly measure this reaction value (Rload), a perpendicular to the loading axis load cell is needed and stress values calculated via equations 1 and 2 (Doyoyo & Wierzbicki 2003):

$$\sigma_{xx} = \frac{Fload}{Area} sin(\alpha) - \frac{Rload}{Area} cos(\alpha) \tag{1}$$

$$\tau_{yx} = \frac{Fload}{Area} cos(\alpha) + \frac{Rload}{Area} sin(\alpha) \tag{2}$$

However, if the material linear elastic properties are known, it is not necessary to measure this reaction force to determine the yield envelope (elastic limit) (Doyoyo & Wierzbicki 2003). Doyoyo & Wierzbicki (2003) derived expressions for shear and normal stresses at the centre of the specimen in the elastic regime using a theoretical and approach combined with finite element analysis, assuming isotropic material:

$$\sigma_{xx} = \left(\frac{\beta_x sin\alpha}{(1-\beta_x)cos^2\alpha + \beta_x} \right) \frac{Fload}{Area} \tag{3}$$

$$\sigma_{yy} = \nu_{xy} \sigma_{xx} \tag{4}$$

$$\tau_{yx} = \left(\frac{cos\alpha}{(\beta_x - 1)sin^2\alpha + 1} \right) \frac{Fload}{Area} \tag{5}$$

Poisson ratio is a relationship between the transverse contraction and the longitudinal strain in the direction of the applied load, while in the linear elastic regime. Even though the samples are non isotropic, the measurements taken via Digital Image Correlation (DIC) allowed to calculate the Poisson ratio (ν) through the following equation 6:

$$\nu_{xy} = -\frac{\varepsilon_{xx}}{\varepsilon_{yy}} \tag{6}$$

For these measurements, the DIC data was obtained for a 90° (tensile load), in which the global coordinate becomes coincident with the local system.

Isotropic materials: Equation 7 indicates the stiffness ratio (β_x) for isotropic specimens with Poisson ratio (ν) (Doyoyo & Wierzbicki 2003; Manaia 2018):

$$\beta_x = \frac{2}{1-\nu} \tag{7}$$

For an isotropic material, the relationship between shear modulus (G) and E is given by:

$$G = \frac{E}{2(1+\nu)} \tag{8}$$

Anisotropic materials: Through equation 9 it is possible to compute the stiffness ratio (β_x) for anisotropic materials, being E_{xx} the Young's modulus, while the G_{xy} is the shear modulus of the specimen for directions x, y;

$$\beta_x = \frac{E_x}{G_{xy}(1 - \nu_{yx}\nu_{xy})} \tag{9}$$

Anisotropic (orthotropic) elasticity theory indicates that through equation 10, it is possible to obtain relationship among these four elastic constants (Volokh 2016):

$$\nu_{xy}E_y = \nu_{yx}E_x \tag{10}$$

Which translates to:

$$\frac{\nu_{xy}}{E_x} = \frac{\nu_{yx}}{E_y} \tag{11}$$

Through these equations, it is possible to verify (considering both VT and VL) if the obtained elastic constants are accurate.

Due to the low stiffness of the test materials, shear (τ_{yx}) and direct stress values (σ_{xx} and σ_{yy}) can be obtained via equations 3 to 5, even with the absence of lateral reaction force loading cell for specific specimen to loading orientations.

Poisson ratios (ν) for H,VT and VL specimens were obtained via digital image correlation during the tensile test configuration of the Arcan setup (α=90°). Considering equations 3 and 5, which are related to tensile and shear stresses, it is possible to conclude that for a tensile test whit the loading angle at 90°, the shear (τ_{xy}) becomes zero, and the component part of the equation 3 that depends on ν/elastic parameters becomes 1. This is and indicator that beyond the modulus, maximum (strength) stress values can be obtained. The same occurs, for different components when the angle is 0° (shear test): σ_{xx} becomes 0, while the angle/component is 1, thus indicating that τ_{xy} can be obtained. The same simplification does not happen for a 45° loading.

Test Procedure

The Arcan test was carried out on an INSTRON® 5900R (Illinois Tool Works Inc. USA) at a displacement rate of 0.5 mm/min with a 5 kN load cell in a controlled environment of 23°C and 50% humidity. Each specimen was tightened using a torque wrench adjusted at 4 Nm for the lateral screws, while the centre clamps were tightened at 8 Nm.

Materials and FFF configurations

FFF specimens were produced using two TronXY X5 (Shenzen TronXY Technology Co. LTD) printers. These are open chamber type machines, capable of a maximum production volume of 210 × 210 × 280 mm^3, reaching extrusion temperatures of 260 °C, and 100 °C for the tray. Two PA12 based 1.75 mm diameter filaments from Fillamentum ©, Parzlich s.r.o (Czech Republic) were used. The first PA12, a pure version, commercially named as Nylon FX256 and the second corresponding to a short fibre reinforced version (Nylon CF15) (Fillamentum 2019b,a) were used. CF15 is reinforced with short carbon fibres with 100 μm length consisting in nearly 15 wt.% of the material, thus being expected a different mechanical behaviour from its unreinforced version, namely increased stiffness. The fibre orientation is aligned with the material deposition direction, following the material flow through the extruder, as shown by Ferreira *et al.* (2019, 2020). Therefore, the fibre disposition matches the printing pattern. Table 1 depicts some of the relevant material properties.

Table 1. Datasheet values and material specifications (Fillamentum 2019b,a).

Property	CF15	FX256
Material density (g/cm^3)	1.08	1.01
Melt flow index ($g/10min$)	14.64	16.56
Glass transition temp. T_g (°C)	44.70	52.91
Thermal conductivity (10^{-3} W/m.k)	144.22	124.82
Tensile strength (MPa)	54.50	45.00
Tensile elastic modulus (MPa)	500	1400
Melting temperature (°C)	160	178
Print temperature (°C)	235-260	235-260

The printing parametrization and slicing methodology were defined with Simplify 3D®, 4.1.1 version, in which the parameters choice was defined considering previous tests, taking into account that the creation of fully dense samples usually leads to printing problems such as warping and bad visual appearance (Fonseca *et al.* 2019). Table 2 depicts the parameters that allowed the best possible printing behaviour. Each batch of samples was produced simultaneously in both machines for CF15 and FX256, being printed six samples (one extra) per batch, according with the orientation. In total, ninety testes were performed (2 materials x 3 build orientations x 3 test orientations x 5 repetitions= 90). Material conditioning was done previously and after to the print process, being each feedstock spool dried during 8h at 70°C in a PrintDry™ (Canada) filament drier. After completing the print process, each set of samples was sealed in plastic bags with silica gel reducing the moisture presence. Once the printing process was completed, all samples with the same building orientation were stored together and posteriorly divided in sets of five.

Table 2. Selected printing parameters.

Extrusion Parameters	
Nozzle diameter (mm)	0.4
Nozzle material	brass/A2 steel
Layer height (mm)	0.2
Number of perimeters per layer	2
Infill percentage (%)	100
Infill pattern (°)	Rectilinear ±45
Skirt outlines	7
Extrusion temperature (°C)	260
Bed temperature (°C)	90
Bed surface	Tempered glass + CUBE®glue
Printing speeds (mm/s)	40

Digital Image Correlation

DIC was used in order to understand how different the deformation fields are for the interest area of each sample. This method allowed to obtain the sample ϵ_{xx}, ϵ_{yy} and ϵ_{xy} (according to the global coordinate system, see Figure 2), making the comparison among distinct samples possible

and to understand which areas were more susceptible to deformation. Considering the vast number of tests, only three, out of five samples, for each building orientation/test direction were prepared for DIC. In order to hide the layer effect and infill patterns, the samples were polished with 320 and 600 grit paper, creating an homogeneous surface required so the speckle can be detected correctly by image correlation. Matte white paint was applied via spray can, while the speckle was created with an Airbrush Iwata CM-B (Anesta Iwata Iberica SL, Barcelona, Spain). A Balser Ace acA2440 (Ahrensburg, Germany) camera was used, Fujifilm Fujinon coupled with a 1:2.3/50 mm (Toquio, Japan) lens, while the image processing was done with VIC-2D Correlated solutions (South Carolina, USA), with a subset size and step of 19 and 7 correspondingly. Images were captured at an acquisition frequency of 2 Hz.

As depicted in Figure 7, small central interest area was considered in the neck portion of the sample, so ϵ_{xx} (longitudinal), ϵ_{yy} (transversal) and ϵ_{xy} (shear) can be obtained. In addition to the localized measurements, the deformation fields were obtained by defining and processing the visible part of the specimen, then converted into strains so the critical areas can be analysed.

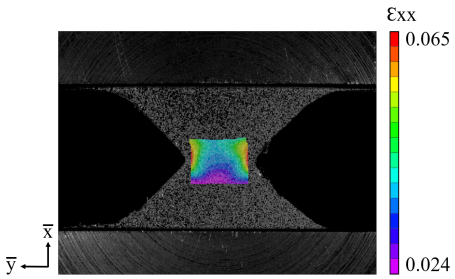

Figure 7. Longitudinal deformation field of a tensile H CF15 sample.

Results and discussion

Experimental curves

Figures 8 through 10 depict the load displacement behaviour of the Arcan testing samples at the different tested loading conditions. Figure 8 presents the behaviour of H printed samples. Considering the shear loading, it is possible to verify that the unreinforced samples sustained lower peak load values; however its displacement was 12.16±1.10 mm, which is significantly higher than observed so far for reinforced samples, that fractured at 3.39±0.25 mm, as it can be proved by the graph from Figure 11. Considering the combined loading, the reinforced material is more capable to exhibit almost similar behaviour for both materials as it can be seen in Figure 11.

Figure 9 represents the test results obtained for the performed to VT samples. It is possible to assert that this printing orientation results in the lowest strength and ductility of all types of samples, for all the loading combinations. This build orientation tests the interlayer behaviour which is weaker. In addition, irregular fracture happened, in some of the cases, outside the neck area, mainly due to printing irregularities.

Figure 10 depicts the curves of the VL samples. It is possible to see that the unreinforced material can sustain higher levels of displacement for the three tests. Considering the load sustained, for shear and combined loading modes, higher ductility values are also obtained with the unreinforced PA version, yet the tensile strength was higher for CF reinforced sample set.

Through the results summary presented in Figure 11a it is possible to verify that even though CF15 is a fibre reinforced material, there is not a relevant gain in terms of strength. It is also possible to verify that H samples present the best overall behaviour. Even though these samples have a bi-directional orientation, unlike the traditional laminate composites in which the tensile strength and stiffness of the fibre is more than ten times higher than the surrounding matrix (da Silva *et al.* 2013), in this particular case, the longitudinal (VL) and transversal performance (VT) is not that different (doubling the force at best). In addition the alternated crossed pattern promotes better adhesion of the adjacent deposed layers since the previous and next layer is 90° rotated, thus improving the overall response of the sample while also promoting a more homogeneous behaviour (close to isotropic). Tensile VT FX256 samples show a higher strength than the reinforced version, which might occur due to the higher material fluidity during the deposition, being more capable to adapt and adhere to the previous layer geometry. This was not reflected for any other testing angle. VT tests indicate that the force needed to promote layer detachment occurred outside the neck area in some of the cases, which might happen due to printing defects. In addition, the similarity in maximum displacement results (between materials) dictates that is the layer interface performance that is being tested, instead of the material by itself (filament). As for VL samples, the deposition lines are oriented in the same direction as the tensile test, being those the best results from the set.

DIC Results

Two approaches were taken considering the DIC analysis. Firstly, a window in the centre of the sample's neck, averaging the strain values for the distinct strain components as mentioned above, reducing the influence of non-desired areas is considered. For the second approach, all of the sample's visible area was selected and processed. This analysis was performed in order to understand which areas of the sample were more appropriate for the evaluation of the elastic properties. Figure 12 depicts the ϵ_{xx} (parallel to loading), ϵ_{yy} (transverse to loading) and ϵ_{xy} (shear) strain fields for the CF15 X samples, since these were the nearest to a homogeneous set of specimens. Figure 12a presents these fields for the tensile test. Longitudinal results indicate that there is no compressing areas, by presenting all positive values, being the notch roots the most critical areas. Transversal strain field (ϵ_{yy}) shows that there is some lateral compression (Poisson effect) in the notch roots, while expansion is observed in the centre of the sample.

For the combined mode results (Figure 12b) it is possible to observe that, in the loading direction, there is expansion of the sample, once again, with the vertices being the most affected areas, thus indicating that the fracture might occur parallel to the grips. It is also shown that lateral compression

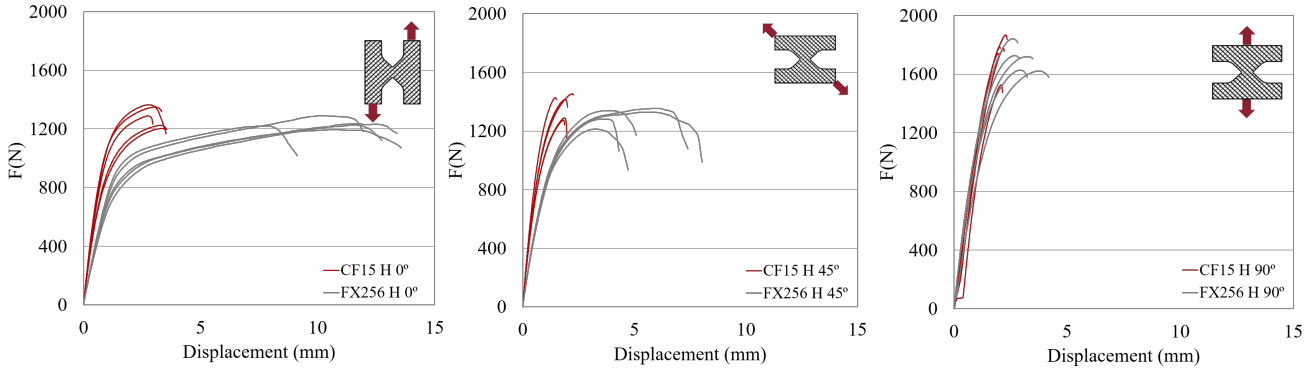

Figure 8. Arcan testing results of H samples at shear, combined mode and tensile loadings.

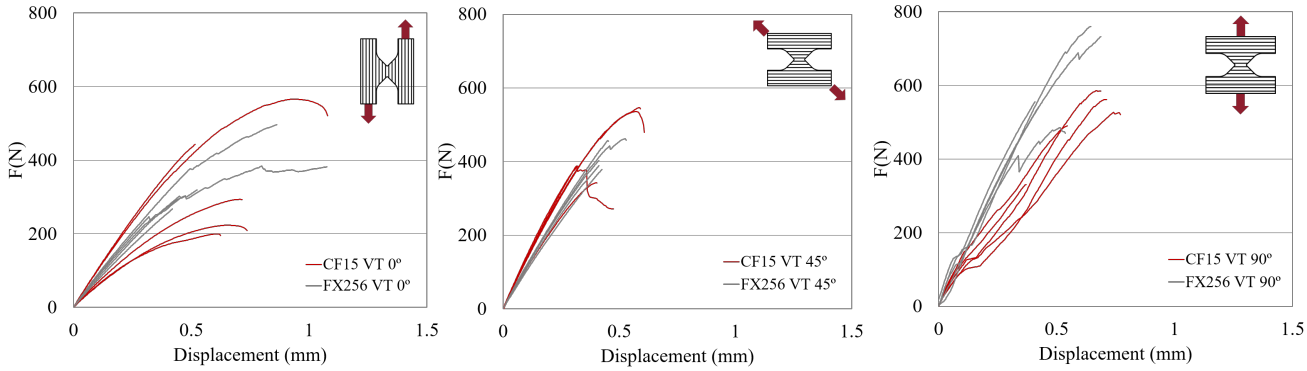

Figure 9. Arcan testing results of VT samples at shear, combined mode and tensile loadings.

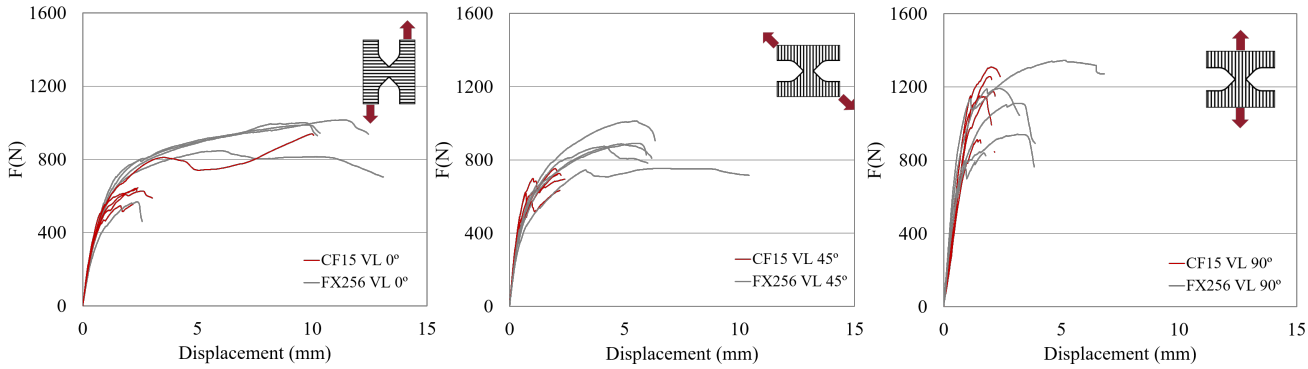

Figure 10. Arcan testing results of VL samples at shear, combined mode and tensile loadings.

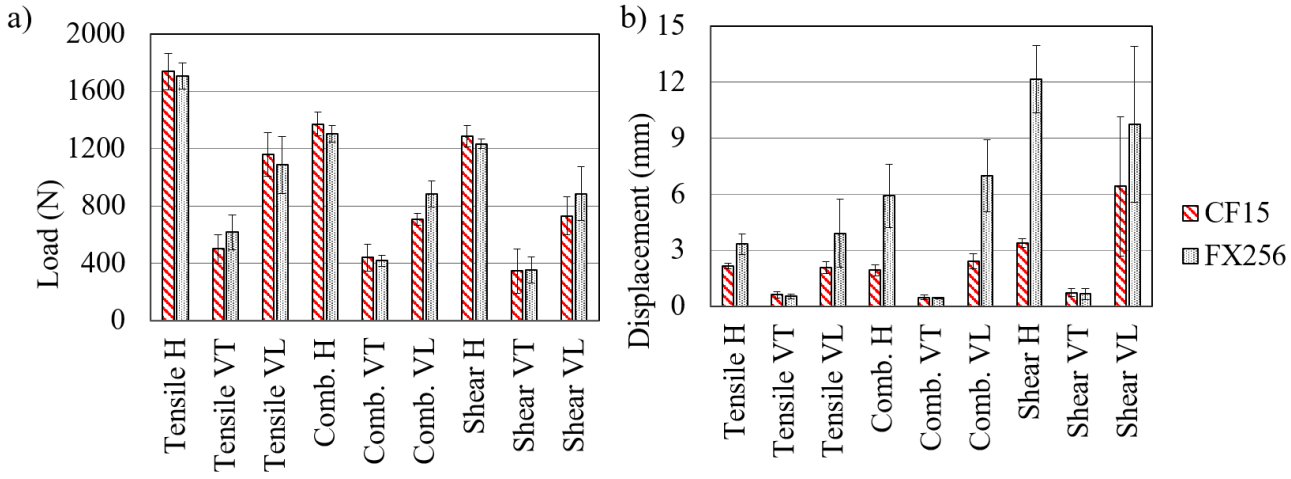

Figure 11. Average test values of (a) maximum load and (b) maximum displacement.

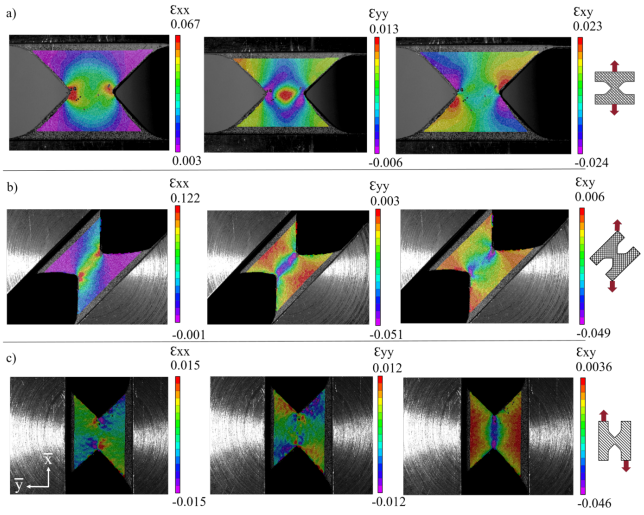

Figure 12. Strain fields: (a) tensile, (b) combined mode and (c) shear for H specimens.

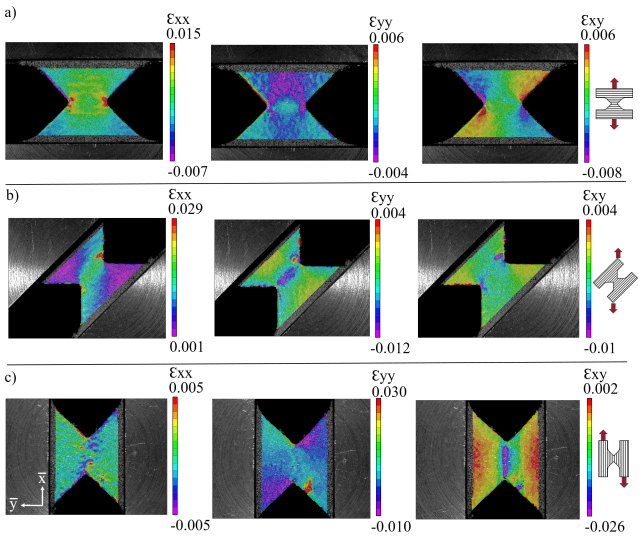

Figure 13. Strain fields: (a) tensile, (b) combined mode and (c) shear for VT specimens.

is generated in the notch area while the rest of the sample is being distended. Figure 12c depicts the shear strain results. It is important to refer that the right grip is static, while the left one is moving upwards. Thus, longitudinal results indicate the presence of compression in the upper part of the sample on both the static side and in the lower part of the moving side. Symmetrical results are observed in the opposite sides. The same effect is found laterally. Shear results evidence high localization values in the ligament of interest.

Considering the VT specimens in Figure 13, it is possible to observe overall lower strain values than for the H samples. This is due to the fact that since the samples have transversal layer deposition, the interlayer performance is being tested instead of the material itself. ϵ_{xx} in Figure 13a indicates that strain concentration points are present in the lateral notches similarly to H specimens, leading to a correct type of fracture in the gauge area; ϵ_{xy} presents similar behaviour to the previous type of sample, however less pronounced. As regards the combined mode results (Figure 13b), it is possible to observe an higher ϵ_{xx} strain out of the section of interest that was responsible for crack nucleation above the gauge area.

From the shear tests (Figure 13c), it is possible to detect a similar behaviour to the H specimens, despite the fact that a point with higher lateral (ϵ_{yy}) strain values in the inferior right part of the arm is detected, indicating a possible fracture nucleation point. Considering the shear strain ϵ_{xy}, it is shown that the central gauge area is the most loaded region of the sample.

Figure 14 depicts the DIC strain fields for the VL specimens. Considering that the most irregular type of fracture was obtained using this type of sample, the strain fields present some explanations, in which for the most samples, the fracture occurred not perpendicularly to the load but in the material deposition direction. For the ϵ_{xx} strain in Figure 14a, it is shown that the critical areas are, once again, the gauge extremities, suffering the most localized strain values. It is shown through ϵ_{yy}, that delamination is prompt to occur in the inferior left arm, since the highest strain values are presented in that point. For the combined mode (Figure 14b), similar nucleation points are observed through both ϵ_{xx} and ϵ_{yy} in the inferior right arm and superior left, which coincide with the ones being pulled as observed in testing. Thus, delamination occurs in the layer direction instead of a gauge fracture.

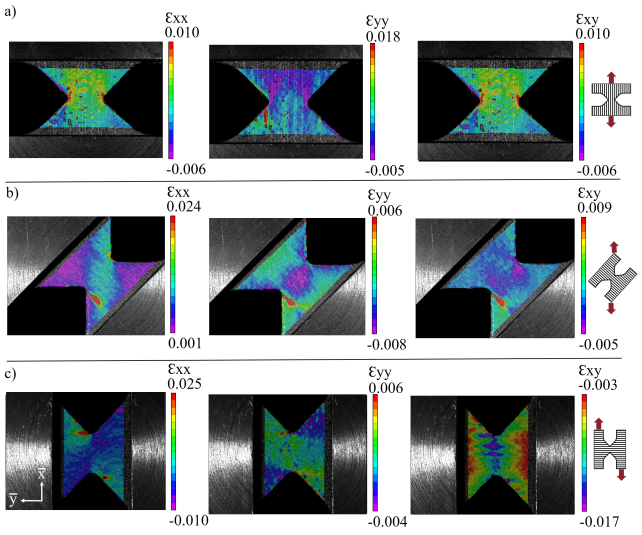

Figure 14. Deformation fields: (a) tensile, (b) combined mode and (c) shear for VL specimens.

The shear test results (Figure 14c) revealed the same trend in which cracking/delamination starts to occur perpendicularly to the gauge, aligned with the deposition. Regarding the shear strain ϵ_{xy}, the effect of delamination becomes clearer since unlike the previous H and VT, that presented higher shear strain values localized consistently in the gauge, in this type of samples, horizontal strain intensification areas indicate that layer detachment are likely to occur.

Fracture analysis

Figure 15 presents the after rupture view of the distinct types of CF15 samples obtained with the DIC setup, thus

complementing the results discussed through DIC strain fields. Throughout the tests it was observed that these failure modes were similar for both materials. For H samples, localization of fracture occurred in the gauge area for all tests independently of loading direction. Only tensile tests presented a clear fracture, while for the combined loading and shear, yielding was observed in the gauge. These specimens orientation exhibited quasi-isotropic behaviour. For VT building orientations irregular fracture was observed. These samples were assumed as the most brittle ones, since the deposition was done parallel to the arms, resulting in a layer interface in the gauge area parallel to the interest line. Through Figure 15 it is possible to observe fractures for tensile and shear. Delamination was found near the section of interest in parallel planes, for the combined mode as indicated in Figure 13b. However, the tests showed that this was not always the case, with the fracture happening also near the grips originated by the printing process. As it can be seen through Figure 16a, VT specimens were produced resorting to support material to provide structural support for the superior arm of the sample.

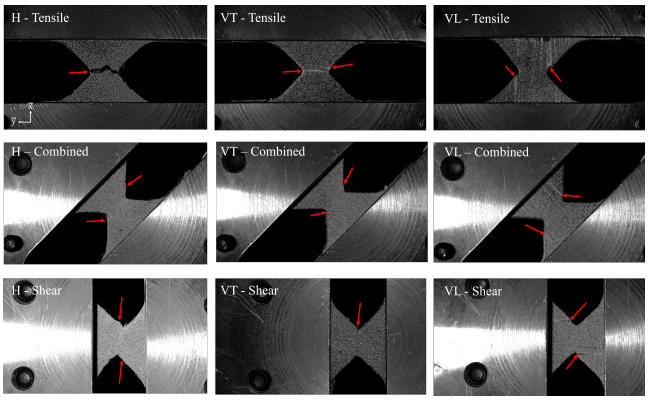

Figure 15. Fracture examples of CF15 for each type of test.

Since there is a gap between the support material and the upper area of the part (simplifying support removal), there is a lack of compression in the arm's first layer, and consequent stress concentration areas due to curved geometry, as presented in Figure 16b. For this reason, some of the unexpected fractures occurred in this area.

VL samples showed delamination of the layers for the distinct loading types. For the tensile tests, in some of the cases, this delamination occurred in the gauge centre, while for the combined mode and shear, the top right and left lower arm were detached from the sample due to the loading direction.

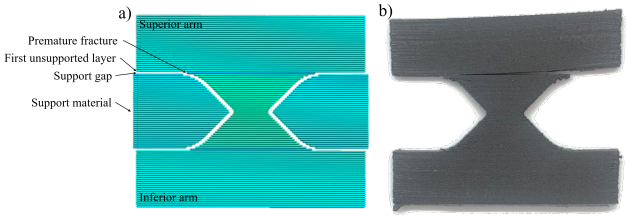

Figure 16. VT specimens: (a) printing scheme and (b) printed fractured sample.

Elastic and strength properties

Considering the three distinct building orientations, H samples, with its alternate $\pm 45^{\circ}$ deposition pattern may be distinguished from the others. H samples generate the nearest to isotropic behaviour, thus being assumed as such in the results analysis. Thus, for verification/comparison purposes, equation 7 can be used. Taking into account, the building type, this sample type could also be analysed by using the composites laminate theory. The other two (VL and VT) can be described as unidirectional, highly anisotropic material, longitudinally and transversally characterized to tensile and shear performance. Therefore, both VL and VT specimens can be considered as one unidirectional material/structure tested in distinct orientations. Figure 17 indicates the different elastic and strength properties evaluated from the proposed tests, assuming the limitations regarding the absence of Rload measurement. From the vertical samples, it is possible to obtain longitudinal and transversal material properties. Taking into account these assumptions, the local coordinate system was adapted according to the deposition (long/transv) as presented in Figure (17b and c). The possibility of printing different orientations with Arcan orientation loadings maximizes the characterization possibilities.

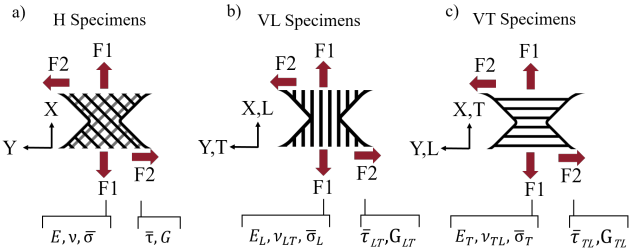

Figure 17. Obtained material properties: (a) H, (b) VL and (c) VT specimens.

By comparing the Poisson coefficient for both materials in Table 3, it is possible to conclude that the use of fibre leads to higher Poisson coefficients. VL samples, in which the material is deposited in the loading direction, present higher Poisson values for CF15. Since the presence of fibre leads to higher stiffness, it is possible to conclude that in order to achieve these high values, lower transversal contractions are also a consequence. Considering that VT samples present low and similar displacements for both materials (even though that ν is obtained in the linear elastic area) it is once again proven that fibre presence grant higher transversal stability. Thus, it is possible to assume that higher Poisson values are obtained in the longitudinal direction (ν_{LT}) rather than in the transversal one (ν_{TL}), and even more pronounced for the reinforced material.

Strength values shown in Table 3 were obtained according to the equations 3 and 5. As previously mentioned, strength and elastic modulus values were calculated for the simple loading modes (shear and tensile), since the stiffness ratio (β_x) dependant component did not present any influential effect. Tensile and shear modulus were calculated by plotting stress by the respective strains values which were obtained via DIC. The combined shear-tensile test results were not considered for this comparison, since the above mentioned

formulation can only be applied during the linear elastic regime for isotropic materials, being the H specimens (assumed as near to isotropic) the only results to be considered.

Considering H samples, it is possible to observe that similarly to the loads in Figure 11a, both materials present analogous results as regards tensile strength, being CF15 slightly higher. Taking into account the shear strength values, once again the reinforced material is superior by a residual advantage. The most notorious difference is presented by the Young's modulus results, being CF15 nearly three times higher than FX256, while the shear modulus is approximately 1.5 lower for the last.

Considering equation 8, shear modulus G was calculated for H samples in order to compare with the experimental results, assuming that the samples presented a quasi-isotropic behaviour. These theoretical values (see equation 8) resulted in 1296.30 MPa and 503.87 MPa, while the experimental values were 597.09±54.54 MPa and 428.37±11.13 MPa for CF15 and FX256 respectively. Thus, it is possible to assess that FX256 presents a more consistent G value, therefore being possible to conclude that the unreinforced material present a more approximate to isotropic behaviour than the CF15, being the fibre the differential factor.

Due to its fabrication nature (deposition orientation), the results obtained from VT and VL specimens can be considered as two components of a unidirectional material like structure. Considering the transversal results (VT), it is possible to see that CF15 presents slightly lower values for all the properties (elastic and strength). However, these results are only indicative on how the interlayer performs, being that in this case, the fibre does not create any influence, since it is deposited with the layers in a perpendicular direction to the fracture. Instead, the difference in values is justified by the polymer intrinsic properties such as the FX256 lower viscosity/higher melt flow index (see table 1) which might promote a better interlayer adhesion.

As regards the VL results, which represent the other component of this material/structure, tensile strength is slightly higher for the reinforced material, while the opposite happens for the shear strength. As expected, the CF15 Young's modulus (even with the high standard deviation) is more than double than FX256, justifiable by the fibre presence. However, the shear modulus presented similar values for both materials, with slight better performance for FX256. Once again, the similarity for this value is associated with the interlayer adhesion, which by analysing ϵ_{xy} from Figure 14c it is possible to observe that the layer effect on the strain is highly pronounced.

Since VT and VL are considered as the same unidirectional material tested in distinct orientations, $G_{LT} \approx G_{TL}$. By analysing the results in Table 3, the approximation is more notorious for the unreinforced material, while the reinforced specimens present a higher G_{LT}. This difference in behaviour may be related to the longitudinal fibre orientation (along with the material deposition).

In addition, according to the orthotropic elasticity theory (Volokh 2016), presented through equation 11, adapted to sample material coordinate system, it is possible to compare

Table 3. CF15 and FX256 strength and elastic properties.

CF15

	$\overline{\sigma}$	$\overline{\tau}$	E	G	ν
H	43.48±3.19	32.16±1.81	3506.08±33	597.09±54.54	0.35
	$\overline{\sigma}_T$	$\overline{\tau}_{TL}$	E_T	G_{TL}	ν_{TL}
VT	12.48±2.52	8.62±3.89	1827.28±288.01	261.22±21.77	0.18
	$\overline{\sigma}_L$	$\overline{\tau}_{LT}$	E_L	G_{LT}	ν_{LT}
VL	29.02±3.82	18.26±3.34	5309.19±798.21	385.16±10.82	0.43
	[MPa]	[MPa]	[MPa]	[MPa]	

FX256

	$\overline{\sigma}$	$\overline{\tau}$	E	G	ν
H	42.68±2.25	30.85±0.88	1169±59.66	428.37±11.13	0.16
	$\overline{\sigma}_T$	$\overline{\tau}TL$	E_T	G_{TL}	ν_{TL}
VT	15.39±3.08	8.81±2.28	1902.34±147.13	383.40±30.85	0.10
	$\overline{\sigma}_L$	$\overline{\tau}_{LT}$	E_L	G_{LT}	ν_{LT}
VL	27.15±5.01	22.10±4.72	1958.28±96.25	390.49±15.54	0.12
	[MPa]	[MPa]	[MPa]	[MPa]	

Table 4. Anisotropic elasticity relationship.

Material	$\frac{\nu_{LT}}{E_L(GPa)}$	$\frac{\nu_{TL}}{E_T(GPa)}$	Difference
CF15	0.10	0.08	0.02
FX256	0.06	0.05	0.01

both V_{LT} and V_{TL} orientations through:

$$\frac{\nu_{LT}}{E_L} = \frac{\nu_{LT}}{E_T} \tag{12}$$

Through the results in Table 4 it is possible to observe that there is an approximate concordance indicating the congruence in separate sets of results (mechanical vs DIC). It is possible to verify once again an higher difference in results for the reinforced material, being this time not possible to relate to the fibre presence since this relationship takes into account the material properties in both directions (transversally and longitudinal). It is, however possible to verify that by approximation, both materials comply with equation 12.

Conclusions

FFF printed parts mechanical performance is considered as the weak point of this technology due to its high anisotropic structure and irregular behaviour. Even considering new and improved engineering polymer specially formulated to the process, both of these problems will remain due to the process intrinsic characteristics.

The scope of this work intends to investigate how differently oriented printed parts react by comparing them, taking into account both reinforced and unreinforced materials. It was proven that in terms of strength, both materials revealed to have unexpected similar responses even though one being the short fibre reinforced version of the other. However, this same reinforcement caused a decrease in terms of ductility confirmed in each variation of the test, thus justifying CF15 higher stiffness levels. It was also proven that FFF parts, regardless of the type of load that they are subjected to, present the worst behaviour in the upright printing orientation (VT samples). In terms of maximum loads sustained, H samples with the $\pm 45^\circ$ infill pattern, proved to be the most capable taking into account the distinct types of single and combined loads, as well as the most regular/repeatable type of fracture.

It can be also assumed that H specimens present a near to isotropic behaviour for the unreinforced samples, while the fibre influence promotes an increased stiffness (E) which is not translated to shear values as expected through the theoretical formula. Finally, through the orthotropic elasticity theory, it is proven the consistency of E_L, E_T, V_{LT} and V_{TL} constants.

Due to its fabrication method in a context of application, FFF parts are hardly ever fully dense printed, which would increase anisotropy levels, particularly in the upright direction, since the inter-facial contact is much lower. Thus, in order to predict this behaviour, this type of study is of major concern.

Acknowledgements

Author gratefully acknowledge the funding of Project POCI-0145-FEDER-016414-FIBR3D-Additive manufacturing based on hybrid processes for long or continuous fibre reinforced polymeric matrix composites, co-financed by Programa Operacional Regional de Lisboa (LISBOA 2020) and by the Project NORTE-01-0145-FEDER-000022 -SciTech, cofinanced by NORTE2020, through FEDER.

References

Ahn, Sung Hoon, Montero, Michael, Odell, Dan, Roundy, Shad, & Wright, Paul K. 2002. Anisotropic material properties of fused deposition modeling ABS. *Rapid Prototyping Journal*, **8**(4), 248–257.

Alfonso, L., Badulescu, C., & Carrere, N. 2018. Use of the modified Arcan fixture to study the strength of bonded assemblies for automotive applications. *International Journal of Adhesion and Adhesives*, **80**(11), 104–114.

Arcan, M., Hashin, Z., & Voloshin, A. 1978. A method to produce uniform plane-stress states with applications to fiber-reinforced materials - A specially designed specimen yields material properties under pure shear or uniform plane-stress conditions. *Experimental Mechanics*, **18**(4), 141–146.

Caminero, M. A., Pavlopoulou, S., López-Pedrosa, M., Nicolaisson, B. G., Pinna, C., & Soutis, C. 2012. Using digital image correlation techniques for damage detection on adhesively bonded composite repairs. *Advanced Composites Letters*, **21**(2), 51–57.

Caminero, M. A., Lopez-Pedrosa, M., Pinna, C., & Soutis, C. 2014. Damage assessment of composite structures using digital image correlation. *Applied Composite Materials*, **21**(1), 91–106.

Casavola, Caterina, Cazzato, Alberto, Moramarco, Vincenzo, & Pappalettere, Carmine. 2016. Orthotropic mechanical properties of fused deposition modelling parts described by classical laminate theory. *Materials and Design*, **90**, 453–458.

Chacón, J. M., Caminero, M. A., García-Plaza, E., & Núñez, P. J. 2017. Additive manufacturing of PLA structures using fused deposition modelling: Effect of process parameters on mechanical properties and their optimal selection. *Materials and Design*, **124**, 143–157.

Choupani, Naghdali. 2008. Experimental and numerical investigation of the mixed-mode delamination in Arcan laminated specimens. *Materials Science and Engineering A*, **478**(1-2), 229–242.

Créac'hcadec, R., Sohier, L., Cellard, C., & Gineste, B. 2015. A stress concentration-free bonded arcan tensile compression shear test specimen for the evaluation of adhesive mechanical response. *International Journal of Adhesion and Adhesives*, **61**, 81–92.

da Silva, Lucas Filipe Martins, Alves, Fernando Jorge Lino, & Marques, António Torres. 2013. *Materiais de Construção*. Publibdustria.

Dias, G. F., de Moura, M. F.S.F., Chousal, J. A.G., & Xavier, J. 2013. Cohesive laws of composite bonded joints under mode I loading. *Composite Structures*, **106**, 646–652.

Doyoyo, Mulalo, & Wierzbicki, Tomasz. 2003. Experimental studies on the yield behavior of ductile and brittle aluminum foams. *International Journal of Plasticity*, **19**(8), 1195–1214.

Ferreira, Isaac, Vale, Diogo, Machado, Margarida, & Lino, Jorge. 2019. Additive manufacturing of polyethylene terephthalate glycol /carbon fiber composites: An experimental study from filament to printed parts. *Proceedings of the Institution of Mechanical Engineers, Part L: Journal of Materials: Design and Applications*, **233**(9), 1866–1878.

Ferreira, Isaac, Madureira, Rui, Villa, Santiago, de Jesus, Abílio M P, Machado, Margarida, & Lino Alves, Jorge. 2020. Machinability of PA12 and short fibre–reinforced PA12 materials produced by fused filament fabrication. *The International Journal of Advanced Manufacturing Technology*. In press: https://doi.org/10.1007/s00170-019-04839-z.

Fillamentum. 2019a. *Nylon CF15 Carbon Material Datasheet*. `https://www.dropbox.com/sh/v7pxxt4kp4bbq0d/AAC2Scjno5kWqnL5IKVtMWDEa/TDS{\_}Nylon{\_}CF15{\_}Carbon.pdf?dl=0`, last accessed 13/9/2019.

Fillamentum. 2019b. *Nylon FX256 Material Datasheet*. `https://www.dropbox.com/sh/v7pxxt4kp4bbq0d/AAC8CNuvZ7ZHUGPjD5dfVUQ{\_}a/TDS{\_}Nylon{\_}FX256.pdf?dl=0`, last accessed 13/9/2019.

Fonseca, J, Ferreira, I A, Moura, M F S F De, Machado, M, & Alves, J L. 2019. Study of the interlaminar fracture under mode I loading on FFF printed parts. *Composite Structures*, **214**(1), 316–324.

Gning, P. B., Delsart, D., Mortier, J. M., & Coutellier, D. 2010. Through-thickness strength measurements using Arcan's method. *Composites Part B: Engineering*, **41**(4), 308–316.

Hachour, K., Zaïri, F., Naït-Abdelaziz, M., Gloaguen, J. M., Aberkane, M., & Lefebvre, J. M. 2014. Experiments and modeling of high-crystalline polyethylene yielding under different stress states. *International Journal of Plasticity*, **54**, 1–18.

Hoffmann, Marco, Zimmermann, Kristian, Bautz, Brian, & Middendorf, Peter. 2015. A new specimen geometry to determine the through-thickness tensile strength of composite laminates. *Composites Part B: Engineering*, **77**, 145–152.

Hung, S. C., & Liechti, K. M. 1997. An evaluation of the arcan specimen for determining the shear moduli of fiber-reinforced composites. *Experimental Mechanics*, **37**(4), 460–468.

Jiang, Delin, & Smith, Douglas E. 2017. Anisotropic mechanical properties of oriented carbon fiber filled polymer composites produced with fused filament fabrication. *Additive Manufacturing*, **18**, 84–94.

Koch, Carsten, Van Hulle, Luke, & Rudolph, Natalie. 2017. Investigation of mechanical anisotropy of the fused filament

fabrication process via customized tool path generation. *Additive Manufacturing*, **16**, 138–145.

Manaia, João P, Pires, Francisco A, de Jesus, Abílio M P, & Wu, Shenghua. 2019. Yield behaviour of high-density polyethylene: Experimental and numerical characterization. *Engineering Failure Analysis*, **97**, 331–353.

Manaia, João P, Pires, Francisco A, de Jesus, Abílio M P, & Wu, Shenghua. 2020. Mechanical response of three semi crystalline polymers under different stress states: Experimental investigation and modelling. *Polymer Testing*, **81**, 106156.

Manaia, João Pedro. 2018. *Deformation Behaviour of Semi Crystalline Polymers under Different Stress States*. Ph.D. thesis, Faculdade de Engenharia Universidade do Porto.

Mohr, D, & Doyoyo, M. 2009. Analysis of the Arcan Apparatus in the. *Journal of Composite Materials*, **36**(22), 2583–2594.

Rybachuk, Maksym, Alice Mauger, Charlène, Fiedler, Thomas, & Öchsner, Andreas. 2017. Anisotropic mechanical properties of fused deposition modeled parts fabricated by using acrylonitrile butadiene styrene polymer. *Journal of Polymer Engineering*, **37**(7), 699–706.

Volokh, Konstantin. 2016. *Anisotropic Elasticity*. Singapore: Springer Singapore. Pages 77–90.

Voloshin, A., & Arcan, M. 1980. Failure of unidirectional fiber-reinforced materials - new methodology and results. *Experimental Mechanics*, **20**(8), 280–284.

Xavier, J., Morais, J., & Pereira, F. 2018. Non-linear shear behaviour of bovine cortical bone by coupling the Arcan test with digital image correlation. *Optics and Lasers in Engineering*, **110**(2), 462–470.

Zou, Rui, Xia, Yang, Liu, Shiyi, Hu, Ping, Hou, Wenbin, Hu, Qingyuan, & Shan, Chunlai. 2016. Isotropic and anisotropic elasticity and yielding of 3D printed material. *Composites Part B: Engineering*, **99**, 506–513.